PAPER
M. Concepción Gimeno, Laura Rodríguez *et al.*
Effect of substituents on the $^1O_2$ production and biological
activity of (N^N^N)Pt(py) complexes

Effect of substituents on the ¹O₂ production and biological activity of (N^N^N)Pt(py) complexes†

Guillermo Romo-Islas,[a,b] María Gil-Moles,[c,d] Arnav Saxena, [ID] [a] Antonio Frontera, [ID] [e] M. Concepción Gimeno [ID] *[c] and Laura Rodríguez [ID] *[a,b]

Twelve (N^N^N)platinum pyridyl complexes, (N^N^N)Pt(pyF), were synthesised and investigated for their singlet oxygen generation and potential biological activities. They exhibited ¹IL and ¹MLCT absorption transitions at approximately 325 and 360 nm, identified through TD-DFT calculations. Luminescence was observed only in the **L¹**-derived compounds in solution, with a dual emission with the main contribution of phosphorescence under deaerated conditions. Room temperature phosphorescence was detected in all solid-state cases. Electron-withdrawing substituents at specific positions (R1 and X) and the number of fluorine atoms in R2 were found to enhance the photosensitizing capabilities of these compounds. Biological assessments, including cytotoxicity and photocytotoxicity, were conducted to evaluate their potential as chemotherapeutic agents and photosensitizers. Complexes with chloro substitution in the N^N^N tridentate ligand of the central pyridine ring exhibited promising chemotherapeutic properties. Ancillary pyridine ring substitution became significant under irradiation conditions, with fluoromethylated substituents enhancing cytotoxicity. Complex **2-CF₃** was the most efficient singlet oxygen producer and a highly effective photosensitizer. CHF₂-substituted complexes also showed improved photosensitizing activity. DNA binding studies indicated moderate interactions with DNA, offering insights into potential biological applications.

Introduction

Coordination and organometallic compounds based on transition metals (TMs) have attracted increasing attention in the last few decades for both fundamental and more applied investigations. In particular, TM complexes (TMCs) with d^8 electronic configuration, *e.g.* Pt(II) or d^{10}, *e.g.* Au(I), are widely explored due to their intrinsic photophysical properties

[a]Departament de Química Inorgànica i Orgànica, Secció de Química Inorgànica, Universitat de Barcelona, Martí i Franquès 1-11, 08028 Barcelona, Spain. E-mail: laurarodriguezr@ub.edu
[b]Institut de Nanociència i Nanotecnologia (IN2UB), Universitat de Barcelona, 08028 Barcelona, Spain
[c]Instituto de Síntesis Química y Catálisis Homogénea (ISQCH), CSIC-Universidad de Zaragoza, Pedro Cerbuna 12, 50009 Zaragoza, Spain. E-mail: gimeno@unizar.es
[d]Departamento de Química, Centro de Investigación de Síntesis Química (CISQ), Universidad de la Rioja, Complejo Científico-Tecnológico, 26004 Logroño, Spain
[e]Departament de Química, Universitat de les Illes Balears, 07122 Palma de Mallorca, Spain

†Electronic supplementary information (ESI) available: NMR and mass spectra of the synthesized compounds. Absorption spectra of the compounds in DMSO. Calculated wavelengths of absorption, transition energies, and oscillator strength. Representation of the NTOs involved in the lowest energy transitions. Emission lifetime decays and residuals. Stability of the compounds in PBS and DMSO (5%) at 37 °C measured by UV-Vis spectroscopy. See DOI: https://doi.org/10.1039/d3dt04050j

ascribed not only to the chemical structure of the ligands but also to the particularity of these metals and their key role in luminescence. These types of luminescent TMCs are currently attracting a great deal of attention for their use as sensors, luminescent markers for bioimaging and catalysts among others.[1–5]

The particularity of these d^8 and d^{10} specific metals is what is called the "heavy atom effect" that favours the intersystem crossing between the S₁ and T₁ excited states. The electrons located at this T₁ level can return to the ground state through different processes, such as radiative processes, giving rise to phosphorescent systems (or those presenting dual emission, fluorescence + phosphorescence). Nevertheless, this emission is frequently quenched by the presence of oxygen, which can be ascribed to energy transfer between the TMC and the oxygen molecules, that is, a triplet, ³O₂, in the ground state. The molecules that produce this energy transfer efficiently are called photosensitizers, PS.

The energy transfer from these PS to the ³O₂ generates singlet oxygen, ¹O₂, that is a highly reactive species (ROS).[6] In fact, the generation of singlet oxygen through a PS is a research area with really increasing interest due to its wide range of versatile applications in several fields such as the synthesis of organic molecules as fine chemicals, pollution control, and photodynamic therapy, or waste treatment of

contaminants.[6–10] Thus, the study of $^1O_2$ production and reactivity has emerged as an important interdisciplinary field.

Some TMCs have been explored as PS, *e.g.* Ru(II) polypyridyl complexes,[11] iridium(III),[12] gold(I) complexes,[13–15] and platinum(II) complexes.[16–19]

Focusing on platinum compounds, it is well known that these types of TMCs have been extensively explored as anticancer drugs since the discovery of cisplatin.[20] However, several toxic side effects such as ototoxicity, nephrotoxicity, and neurotoxicity of cisplatin have been detected during the illness treatment and some improvements are strongly required. In order to overcome these drawbacks, phototherapy (also called photodynamic therapy, PDT) has emerged as a non-invasive and controllable strategy for precise tumour ablation.[21] PDT requires the use of a PS able to transform the oxygen present in the environment into cytotoxic $^1O_2$ upon irradiation with light. This causes the destruction of organelles and leads to cancer cell death. The presence of the Pt heavy atom, which is suitable to populate the T_1 excited state, makes Pt(II) compounds adequate to potentially react with $^3O_2$. Hence, the well-known anticancer activity of Pt(II) compounds together with their potential behaviour as PS make them suitable candidates to be explored not only as anticancer drugs but also to analyse the effect of light to generate a Pt(II) PS with improved anticancer activity.

There is still a lot to be explored in this field, mainly if we take into consideration that small variations in the chemical structure of the Pt(II) compounds can significantly impact their resulting photophysical properties. This will affect the T_1 population and the energy transfer process with oxygen. For this reason, in this work we have designed and synthesized different series of Pt(II) compounds, which feature a N^N^N tridentate ligand driving the planar geometry of the complexes and incorporating a pyridyl ligand at the fourth coordination position. Small variations have been introduced both in the chemical structure of the N^N^N ligand and in the pyridyl group to gain insight into the factors that can affect the photophysical properties, singlet oxygen production and biological activity of the compounds. Fluorine ligands have been considered in this work, as previous studies have shown that incorporating these atoms into the structure of the compounds significantly enhances biological activity in potential anticancer drugs.[22] The introduction of several numbers of fluorine atoms can be easily performed through the selected pyridyl ligands, which is a direct tool to evaluate the effect of fluorine ligands on the biological activity of the studied compounds. Therefore, this systematic study holds great relevance for understanding and designing promising new drugs that can serve both as chemotherapeutic agents and PS in PDT.

Results and discussion

Synthesis and characterization

The synthesis of the (N^N^N)platinum pyridyl complexes (from now on, (N^N^N)Pt(pyF)) was carried out following the different steps displayed in Scheme 1. The synthesis of the bis (triazole) N^N^N $\mathbf{H_2L^1}$–$\mathbf{H_2L^4}$ ligands and [Pt(DMSO)(L)] precursors was recently reported by us.[23] The [Pt(DMSO)(L)] compounds were reacted with the p-R$_2$-pyridyl ligand (R$_2$ = CF$_3$, CHF$_2$ and CH$_3$) to obtain the final products in moderate to high yields (45–85%).
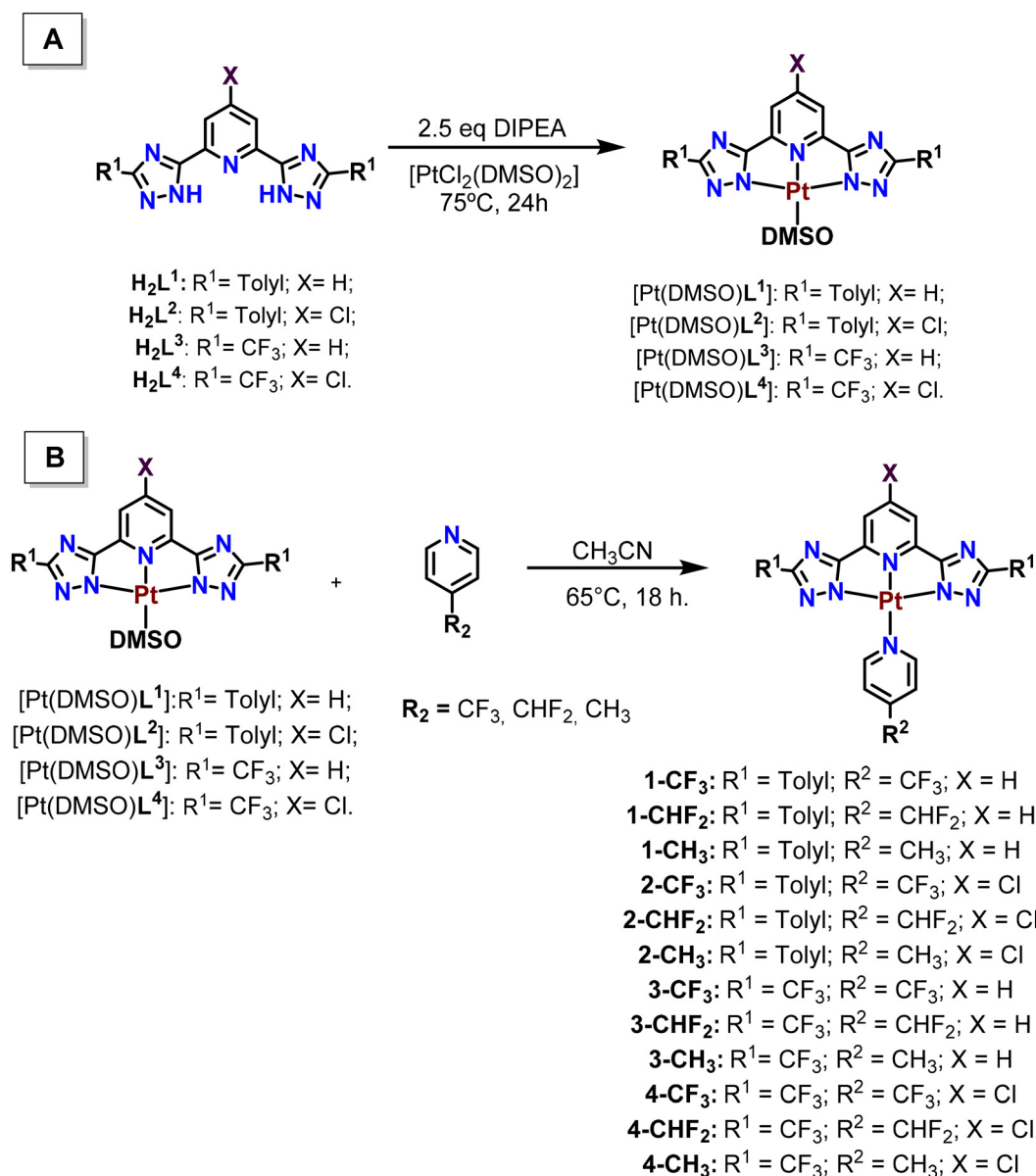
The ^{1}H NMR spectra of the final products show the presence of the corresponding protons of the pyridyl groups that are 0.40–0.23 ppm downfield shifted with respect to the [Pt (DMSO)L] precursors. A triplet centered at 6.95–6.65 ppm, which corresponds to the hydrogen atom of the –CHF$_2$ substituent of the pyridine ligand, can also be observed for the x-CHF$_2$ (x = **1**–**4**) compounds. The signals corresponding to the –CF$_3$ and –CHF$_2$ moieties are also detected in the ^{19}F NMR spectra of the corresponding compounds and in their IR spectra with a well-defined vibration band between 1183 and 1061 cm^{-1} corresponding to the ν(C–F). The final evidence of the correct formation of the compounds has been obtained from the high-resolution mass spectra with the identification of the molecular peaks corresponding to [M + H$^+$] or [M + Na$^+$].

Photophysical characterization

Absorption and emission spectra of the compounds were recorded in 10^{-5} M DMSO solutions at room temperature. DMSO was chosen for analogy to the biological assays performed with these compounds (see below), although we are aware that it is not the best option for recording absorption spectra due to the long wavelength cut-off of this solvent that hinders the main absorption transitions in the ground state. Low-intensity absorption bands at around 325 and 360 nm were recorded for all the compounds (Table 1) that have been assigned to ^{1}IL and ^{1}MLCT transitions as reported and studied for similar compounds in the literature.[23–32]

TD-DFT calculations were performed on all complexes to further support the band assignments. We have calculated the first 20 excited states using the CAM-B3LYP/def2-TZVP level of theory in DMSO treated as a continuum model. The results are shown in Fig. 1 for **1-CF$_3$** as an exemplifying compound and Table S1† as well as Fig. S39–S49† for the rest of the compounds. The two lowest and detectable energy bands of compound **1-CF$_3$** correspond to the $S_0 \rightarrow S_1$ excitation (λ_{exc} = 376 nm, 3.298 eV, f = 0.0170) and the $S_0 \rightarrow S_2$ excitation (λ_{exc} = 305 nm, 4.060 eV, f = 0.0160). These values are in reasonable agreement with the experimental values (365 and 324 nm). For convenience and simplicity, the natural transition orbitals (NTOs) have been computed and represented in Fig. 1 to provide a qualitative description of the electronic transitions. The $S_0 \rightarrow S_1$ excitation consists of one NTO pair (98%) with the highest occupied transition orbital (HOTO) located at the metal center and the tridentate ligand. The lowest unoccupied transition orbital (LUTO) is mainly located in the tridentate ligand, thus revealing that the lowest energy band is a mixture of metal–ligand and inter-ligand charge transfer. The second band corresponds to the $S_0 \rightarrow S_2$ excitation consisting mainly of two NTO pairs (other less dominant NTO pairs have been omitted). The most dominant NTO pair (70%) is basically

A

H_2L^1: R^1= Tolyl; X= H;
H_2L^2: R^1= Tolyl; X= Cl;
H_2L^3: R^1= CF$_3$; X= H;
H_2L^4: R^1= CF$_3$; X= Cl.

2.5 eq DIPEA
[PtCl$_2$(DMSO)$_2$]
75°C, 24h

[Pt(DMSO)L^1]: R^1= Tolyl; X= H;
[Pt(DMSO)L^2]: R^1= Tolyl; X= Cl;
[Pt(DMSO)L^3]: R^1= CF$_3$; X= H;
[Pt(DMSO)L^4]: R^1= CF$_3$; X= Cl.

B

[Pt(DMSO)L^1]:R^1= Tolyl; X= H;
[Pt(DMSO)L^2]: R^1= Tolyl; X= Cl;
[Pt(DMSO)L^3]: R^1= CF$_3$; X= H;
[Pt(DMSO)L^4]: R^1= CF$_3$; X= Cl.

R_2 = CF$_3$, CHF$_2$, CH$_3$

CH$_3$CN
65°C, 18 h.

1-CF$_3$: R^1 = Tolyl; R^2 = CF$_3$; X = H
1-CHF$_2$: R^1 = Tolyl; R^2 = CHF$_2$; X = H
1-CH$_3$: R^1 = Tolyl; R^2 = CH$_3$; X = H
2-CF$_3$: R^1 = Tolyl; R^2 = CF$_3$; X = Cl
2-CHF$_2$: R^1 = Tolyl; R^2 = CHF$_2$; X = Cl
2-CH$_3$: R^1 = Tolyl; R^2 = CH$_3$; X = Cl
3-CF$_3$: R^1 = CF$_3$; R^2 = CF$_3$; X = H
3-CHF$_2$: R^1 = CF$_3$; R^2 = CHF$_2$; X = H
3-CH$_3$: R^1= CF$_3$; R^2 = CH$_3$; X = H
4-CF$_3$: R^1 = CF$_3$; R^2 = CF$_3$; X = Cl
4-CHF$_2$: R^1 = CF$_3$; R^2 = CHF$_2$; X = Cl
4-CH$_3$: R^1 = CF$_3$; R^2 = CH$_3$; X = Cl

Scheme 1 Synthetic procedure to obtain the (N^N^N)Pt precursors (A) and (N^N^N)Pt(pyF) complexes (B).

Table 1 Photophysical data of the (N^N^N)Pt(pyF) compounds in 10⁻⁵ M DMSO solutions

Compound	A (ε, 10^3 cm^{-1} m^{-1})	λ_{max} Em (nm)
1-CF$_3$	324 (30.0), 365 (10.3)	452, 536
1-CHF$_2$	324 (29.1), 365 (9.5)	445, 536
1-CH$_3$	324 (29.5), 365 (10.0)	425, 536
2-CF$_3$	322 (13.4)	
2-CHF$_2$	322 (12.6)	
2-CH$_3$	322 (11.2)	
3-CF$_3$	342 (17.5)	
3-CHF$_2$	342 (10.6)	
3-CH$_3$	342 (9.9)	
4-CF$_3$	361 (8.0)	
4-CHF$_2$	312 (22.1), 361 (7.3)	
4-CH$_3$	312 (26.6), 361 (12.2)	

formed due to an electron transfer from the d_{z^2} orbital of Pt (HOTO) to a σ*(Pt–N) antibonding orbital (LUTO) that covers the whole PtN$_4$ core (see Fig. 1). The second pair of the S$_0$ → S$_2$ excitation (17%) is very similar to the one observed in the S$_0$ → S$_1$ excitation, where the "hole" orbital is localized at the Pt atom and the tridentate ligand and the "electron" orbital is localized mainly in the pyridine moiety of the tridentate ligand.

The emission spectra of all compounds were also recorded under the same conditions upon excitation of the samples at 330 nm. We have observed that only the compounds derived from L^1 (**1-CF$_3$**, **1-CHF$_2$** and **1-CH$_3$**) display significant luminescence in solution and dual emission (fluorescence + phosphorescence bands, Fig. 2A). Phosphorescence emission is
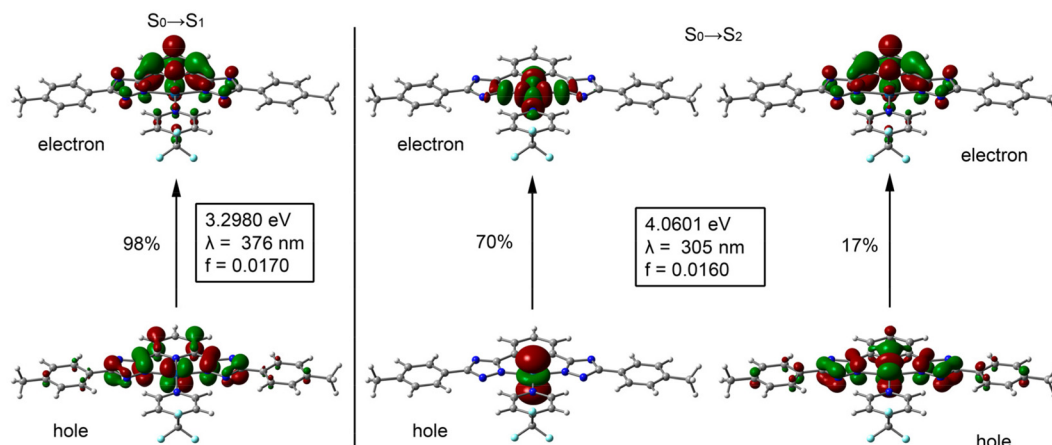
Fig. 1 Representation of the NTOs involved in the $S_0 \rightarrow S_1$ (left) and $S_0 \rightarrow S_2$ (right) excitation of compound **1-CF$_3$**, with indication of the theoretical λ_{exc}, oscillator strength and relative contribution of each NTO pair.
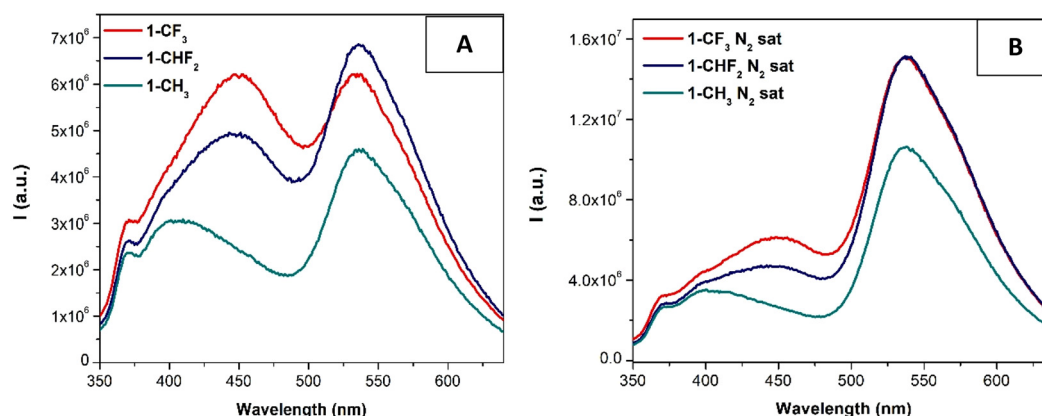

Fig. 2 Emission spectra of compounds **1-CF$_3$**, **1-CHF$_2$** and **1-CH$_3$** in 10^{-5} M air-eq. (A) and N$_2$ sat. (B) DMSO solutions (λ_{exc} = 330 nm), respectively.

clearly predominant when oxygen is removed from the solutions (Fig. 2B). The corresponding excitation spectra collected at *ca.* 550 nm (see the ESI†) display in all cases two bands, one centered at 330 nm corresponding to ^{1}IL/^{1}MLCT transitions and another one of weaker intensity at *ca.* 420 nm, which may be ascribed to the formation of some aggregates, as previously observed for the [Pt(N^N^N)(diphos)] complexes recently reported by us based on previous data reported in the literature.[23] The corresponding emissions are ascribed to metal perturbed ^{1}IL/^{1}MLCT transitions and ^{3}MLCT/^{3}MMLCT transitions.[23–32] The influence of the apparent innocent chlorine substituent on the resulting emission responsible for the quenching recorded for **L^2**-derivatives was also previously observed for other analogous Pt(N^N^N) complexes.[23]

The corresponding emission quantum yields corresponding both to the fluorescence and to the phosphorescence band were recorded with low values of 1–2% for the fluorescence being about double for the phosphorescence emission (Table 2). As expected, the latter value, the phosphorescence quantum yield, increases in the absence of oxygen up to *ca.* 4%. Emission lifetimes were also measured for the fluo-

Table 2 Emission quantum yields (Φ) and lifetimes (τ) of the compounds in 10^{-5} M DMSO solutions

Compound	Φ_{fl} (air-eq./ N$_2$ sat.)	τ (air-eq./ N$_2$ sat., ns)	Φ_{phos} (air-eq./ N$_2$ sat.)	τ (air-eq./ N$_2$ sat., μs)
1-CF$_3$	0.01/0.01		0.02/0.03	0.77/1.26
1-CHF$_2$	0.01/0.01		0.02/0.04	0.53/1.23
1-CH$_3$	—/—		0.02/0.04	0.47/1.08

rescence band using a band-pass filter of 420 nm and the obtained values of 1.59–2.57 ns agree with a singlet origin transition. In the same way, the phosphorescence radiative decay times were collected using a band-pass filter of 550 nm obtaining lifetime values in the range of 0.5–1.2 μs that, together with a large Stokes' shift, agree with a triplet state origin emission band (phosphorescence). A point to retain is that, according to the values in Table 2, the substituent of the pyridyl ligand does not seem to affect substantially the resulting photophysical properties of the compounds, and just a

small effect on the fluorescence is observed that is less favoured for the *p*-methyl substituted pyridyl ligand (**1-CH₃**).

The radiative (k_r) and non-radiative (k_{nr}) rate constants were retrieved from the corresponding emission lifetimes and QY values and the results are displayed in Table 3.

With these values we can affirm that the increase in the quantum yields and emission lifetimes in deoxygenated samples is due to a decrease in the non-radiative processes, as reflected in the lower values of k_{nr} in nitrogen saturated samples, while the radiative processes, reflected in the k_r values, are not substantially affected by the presence of oxygen in the solutions. This relevant information encouraged us to analyze the potential use of our systems in the energy transfer process from the populated triplet excited states to the triplet ground state of the dioxygen molecule (see below). In the event

of success, our compounds may be of potential interest in acting as photosensitizers.

Interestingly, the emission properties of the compounds were improved in the solid state since almost all of them (except those derived from the **L²** ligand) are emissive in this medium (see Fig. 3 and Table 4).

In general, the emission in the solid state depends slightly on the *para*-substituted pyridyl ligands, except for the cases of **1-CH₃** and **4-CF₃**, where the compounds display the most red-shift compared to the other two complexes of the same series. This can be due to more efficient packing that favors Pt···Pt and/or π···π or Pt···π contacts. In the first case, this packing can be more favored due to the presence of lower bulky and more planar substituents (X = H, R₁ = *p*-tolyl and R₂ = CH₃), while the presence of all the electron-withdrawing substituents in **4-CF₃** can be the reason for this more efficient packing due to the resulting lower electron density at the Pt center that can be compensated by these intermolecular contacts. Regarding this, the series derived from **L⁴** (**4-CF₃**, **4-CHF₂** and **4-CH₃**) displays a more red-shifted emission wavelength with respect to the other complexes. We must remember that this series contains electron-withdrawing substituents at the N^N^N ligand (X = Cl and R₂ = CF₃), supporting the direct relationship between the deficient electron density and the recorded red-shift.

Table 3 Radiative (k_r) and non-radiative (k_{nr}) constants of the compounds in solution considering the phosphorescence emission

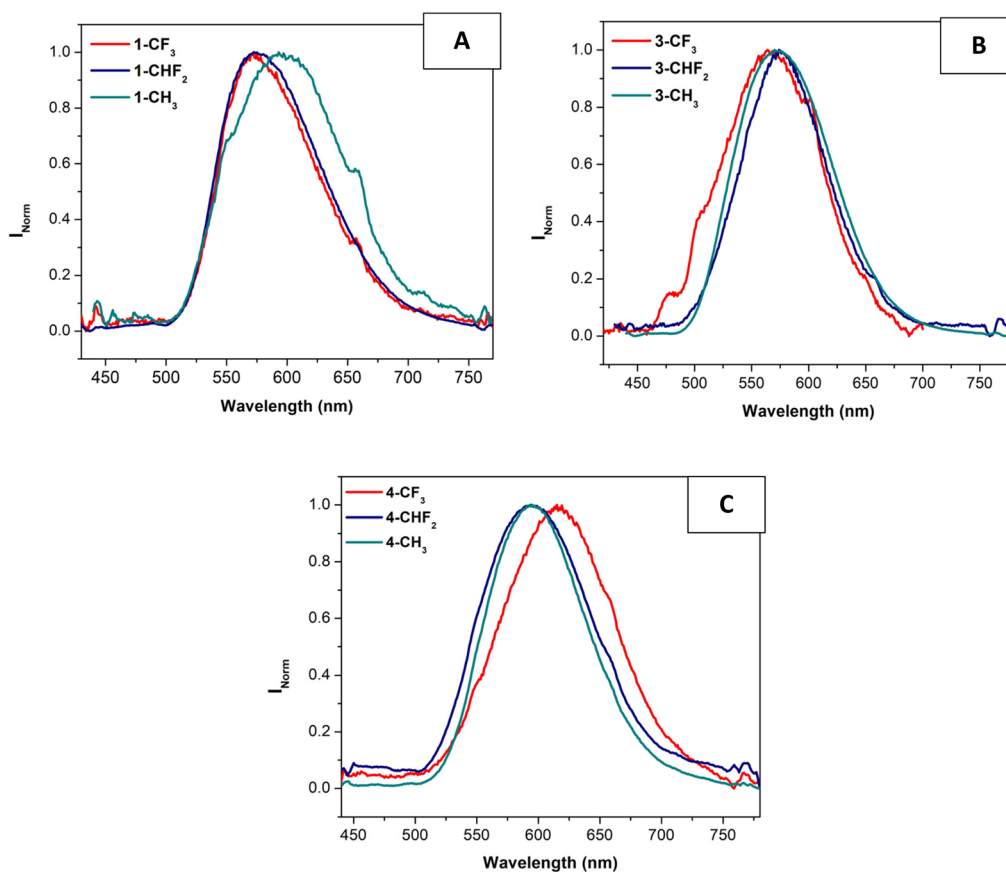| Complex	k_r (air-eq.) × 10^5 s⁻¹	k_{nr} (air-eq.) × 10^5 s⁻¹	k_r (N₂ sat.) × 10^5 s⁻¹	k_{nr} (N₂ sat.) × 10^5 s⁻¹
1-CF₃	0.26	12.70	0.24	7.70
1-CHF₂	0.38	18.50	0.32	7.80
1-CH₃	0.42	20.90	0.37	8.89

Fig. 3 Normalized emission spectra of compounds *x*-CF₃, *x*-CHF₂ and *x*-CH₃ (*x* = 1, A; *x* = 3, B and *x* = 4, C) in the solid-state (λ_{exc} = 400 nm).

Table 4 Photophysical data of compounds *x*-CF₃, *x*-CHF₂ and *x*-CH₃ (*x* = **1**, A; *x* = **3**, B and *x* = **4**, C) in the solid state (λ_{exc} = 400 nm)

Complex	λ_{max} Em (nm)	Φ	τ (µs)	χ^2	k_r (× 10⁵ s⁻¹)	k_{nr} (× 10⁵ s⁻¹)
1-CF₃	573	0.01	0.38	1.2	0.3	26.0
1-CHF₂	575	0.01	0.69	1.2	0.2	14.3
1-CH₃	598	0.01	0.34	1.1	0.3	29.1
3-CF₃	569	0.004	0.40	1.1	0.1	24.9
3-CHF₂	578	0.003	0.29	1.3	0.1	34.4
3-CH₃	572	0.02	0.28	1.1	0.5	35.2
4-CF₃	618	0.005	0.23	1.1	0.2	43.3
4-CHF₂	595	0.02	0.20	1.0	1.0	49.0
4-CH₃	595	0.01	0.15	0.8	0.9	65.8

The origin of these emission bands has been attributed to ³MMLCT transitions.[24,28,29,31–36] The recorded emission quantum yields are on the same order as those previously recorded in solution while the emission lifetimes are slightly shorter and on the order of hundreds of nanoseconds (0.15–0.69 µs), supporting the triplet origin of the emission (see the ESI†).

The lower lifetime values recorded in the solid state compared to those in solution can be due to the more favored non-radiative processes (k_{nr} values in Table 4) since the radiative deactivation pathways (k_r values in Table 4) are quite close to those recorded previously in solution (Table 3).

Singlet oxygen production

As stated above, the phosphorescence emission of the compounds in solution is clearly affected by the presence of oxygen and this was an initial motivation to analyze their potential to react with O₂ (that is, a triplet in the ground state) to produce singlet oxygen, ¹O₂, with potential applications as photosensitizers, PS. The experiments were carried out in dichloromethane where the concentration of oxygen can be higher in order to obtain a more rigorous analysis of the calculated singlet oxygen production quantum yields, Φ_Δ, and using perinaphthenone as a reference. The obtained results are shown in Table 5.

The obtained data are in the range 12–42%, being the majority in the top-range order compared to other values previously reported in the literature for Pt(ɪɪ) PS.[23,37–41] We can observe that in this case, the R₂ substituent at the pyridyl ligand does affect the resulting Φ_Δ but some trends can be

Table 5 ¹O₂ production quantum yields (Φ_Δ) of the (N^N^N)Pt(pyF) compounds in air-equilibrated dichloromethane solutions (λ_{exc} = 350 nm)

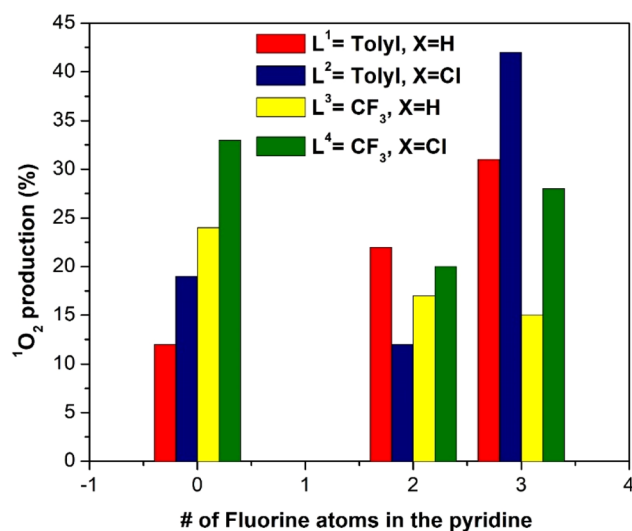| Complex	Φ_Δ (%)	Complex	Φ_Δ (%)
1-CF₃	31	**3-CF₃**	15
1-CHF₂	22	**3-CHF₂**	17
1-CH₃	12	**3-CH₃**	24
2-CF₃	42	**4-CF₃**	28
2-CHF₂	12	**4-CHF₂**	20
2-CH₃	19	**4-CH₃**	33

found. The R₂ = CF₃ substituent improves the behaviour of the compound as PS in the **1** and **2**-series with R₁ = *p*-tolyl. In contrast, when the N^N^N ligand is electron deficient with R₁ = CF₃, the best ¹O₂ production is recorded for the methyl substituted pyridyl ligands (R₂ = CH₃). Additionally, the chloride substituent at the N^N^N ligand (X = Cl) led to a general increase of the Φ_Δ. A higher population of the T₁ triplet excited state in the chlorinated derivatives may be the reason for a more effective energy transfer to the triplet state of the oxygen, thus allowing the formation of this ¹O₂ reactive species.

We can also observe that there is not a direct correlation between the number of fluorine atoms in R₂ and the resulting Φ_Δ. However, in the case of the compounds with R₂ = CH₃ (that is, with zero fluorine atoms at the pyridyl ligand), we can observe a clear increase in the production of singlet oxygen, following the **L⁴** > **L³** > **L²** > **L¹** trend. Hence, there is some influence of the presence of electron-withdrawing substituents at the R₁ and X positions of the complex structure on the production of singlet oxygen. Finally, the number of fluorine atoms in R₂ with those complexes without electron-withdrawing substituents at the N^N^N ligand (red bars in Fig. 4) improves the behavior of the compounds as PS (higher Φ_Δ).

Biological assays

Cytotoxicity and phototoxicity. The stability of the complexes in biological media (phosphate buffer solution, PBS, with 5% DMSO at 37 °C) was measured through UV-Vis spectra. The spectra were recorded at 0, 24, 48, and 72 hours, and all of them indicated that the platinum complexes remained stable in solution throughout this period (see Fig. S63–S69†).

The initial phase of investigating the biological potential of these compounds involved conducting *in vitro* bioactivity assessments through MTT-reduction assays. A549 cells, a human non-small cell lung cancer cell line, were exposed to

Fig. 4 Plot of singlet oxygen production quantum yield, Φ_Δ, of the (N^N^N)Pt(pyF) complexes as a function of the N^N^N ligand and the pyridine used.

various platinum complexes under different conditions to evaluate their potential as both chemotherapeutic agents (tested in the absence of light) and photosensitizers (under photoactivation). The results obtained are presented in Table 6. For comparison purposes the reference compound for cancer treatment, cisplatin, has been included and measured at 72 h.[42]

In the absence of light, only complexes **2-CF₃**, **2-CHF₂**, and **2-CH₃**, which were incubated for 72 hours, demonstrated cytotoxic activity. Given the efficiency of these complexes as singlet oxygen generators, they were subjected to testing under irradiation at 405 nm under two distinct conditions. Initially, cells were incubated with the complexes for 24 hours, followed by 10 minutes of irradiation, and then allowed to incubate for a total of 72 hours. Under these conditions, only complexes **2-CF₃** and **2-CHF₂** improved their activity with a phototherapeutic index of 6.9 and 5.9, respectively, exhibiting IC₅₀ values in the low micromolar range. In a second experiment, the cells were incubated with the complexes for 1 hour, followed by 10 minutes of irradiation, and then left to incubate for a total of 72 hours. Under these conditions very similar values were obtained for the initially active complexes, and some of the previous inactive complexes, such as complexes **1-CHF₂**, **4-CHF₂** and **4-CH₃**, began to exhibit moderate activity.

In an attempt to establish a structure–activity relationship, it appears that within the N^N^N tridentate ligand, both the chloro substituent in the *para* position of the central pyridyl group and the tolyl substituent in the triazole ring enhance activity, as only the family series **2** exhibited activity. However, the substitution in the ancillary pyridine ligand with either methyl or fluoromethylated groups does not seem to be critical for activity. Nevertheless, under irradiation conditions, this pyridine ring substitution becomes more significant. Only the fluoromethylated species improved cytotoxicity, although making a direct comparison with singlet oxygen production is not straightforward. Complex **2-CF₃** is the highest singlet oxygen producer and has one of the highest phototherapeutic indices, while complex **2-CHF₂** is not, but it still shows a high PI. Independently, the CHF₂-substituted complexes appear to be the most effective in enhancing activity as photosensitizers.

In summary, it can be asserted that the generation of singlet oxygen is not the sole determinant of cytotoxicity. While not all complexes demonstrate cytotoxicity, it is evident that the increased production of singlet oxygen enhances their overall activity. Consequently, the observed activity of these complexes represents a synergistic blend of both chemotherapy and photodynamic therapy.

DNA-binding

In order to know the potential biological target of these platinum complexes and in view of the fact that DNA is the preferred target for platinum complexes, we investigated the DNA binding of some of the complexes.

Absorption spectral titration experiments were performed at a constant concentration of Pt complexes (**1-CF₃**, **2-CF₃**, **3-CF₃**, and **4-CF₃**) of 20 μM, while the concentration of calf thymus CT-DNA ranged from 0 to 200 μM. The absorbance (A) of the complex's most significantly affected band was measured after incremental additions of CT-DNA. To eliminate absorbance attributable to DNA at the specific wavelength, a reference cell containing DNA and a solvent mixture of 1% DMSO and PBS buffer at pH 7.4 was employed. Utilizing the data obtained from the absorption titration, we calculated the binding constant (K_b) of the Pt(II) complexes with CT-DNA, applying the Wolfe–Shimer equation:

$$\frac{[\text{DNA}]}{(\varepsilon_a - \varepsilon_f)} = \frac{[\text{DNA}]}{(\varepsilon_a - \varepsilon_f)} + \frac{1}{K_b(\varepsilon_b - \varepsilon_f)}$$

In this analysis, we used various coefficients to describe the spectral changes observed. Specifically, ε_a represents A/[Pt(II) complex], ε_f stands for the extinction coefficient of the free Pt(II) compound, and ε_b signifies the extinction coefficient of the fully bound platinum(II) complex. By plotting $[\text{DNA}]/(\varepsilon_a - \varepsilon_f)$ against [DNA], we can determine K_b as the ratio of the slope to the intercept. The calculated K_b values are detailed in Table 7.

Fig. 5 provides visual insight into the UV-vis spectra generated by the incremental addition of DNA to the solutions of **1-CF₃**, **2-CF₃**, **3-CF₃**, and **4-CF₃**. In all cases, a reduction in the intensity of the entire wavelength range is observed, and, in some instances, a subtle red shift is evident. This red shift may suggest that the complexes interact with the DNA through an intercalation mode.

When the complex–DNA interaction occurs *via* intercalation, it likely involves weak interactions between the ligand and the DNA base pairs. This combination of π electrons from the compound and the π electrons from the DNA nitrogenous

Table 6 IC₅₀ values of Pt(II) complexes in the dark and under 405 nm

Complex	IC₅₀ dark	IC₅₀ 405 nm (24 h)	IC₅₀ 405 nm (1 h)	PI[a]
1-CF₃	>50	>50	>50	—
1-CHF₂	>50	>50	28.88 ± 3.05	>2
1-CH₃	>50	>50	>50	—
2-CF₃	14.61 ± 2.26	2.1 ± 1.17	2.33 ± 1.76	6.9
2-CHF₂	11.36 ± 0.17	1.92 ± 0.51	1.51 ± 0.89	7.5
2-CH₃	2.95 ± 0.21	2.85 ± 0.46	3.03 ± 0.74	1
3-CF₃	>50	>50	>50	—
3-CHF₂	>50	>50	>50	—
3-CH₃	>50	>50	>50	—
4-CF₃	>50	≈50	>50	—
4-CHF₂	>50	>50	36.13 ± 3.25	>2
4-CH₃	>50	>50	39.70 ± 8.94	>2
Cisplatin	1.9 ± 0.8	—	—	—

[a] Best conditions.

Table 7 DNA binding constants for complexes **1-CF₃**–**4-CF₃**

Complex	K_b
1-CF₃	1.87×10^4
2-CF₃	1.08×10^4
3-CF₃	6.78×10^3
4-CF₃	—[a]

[a] Non-linear response; hence, it was not possible to determine K_b.
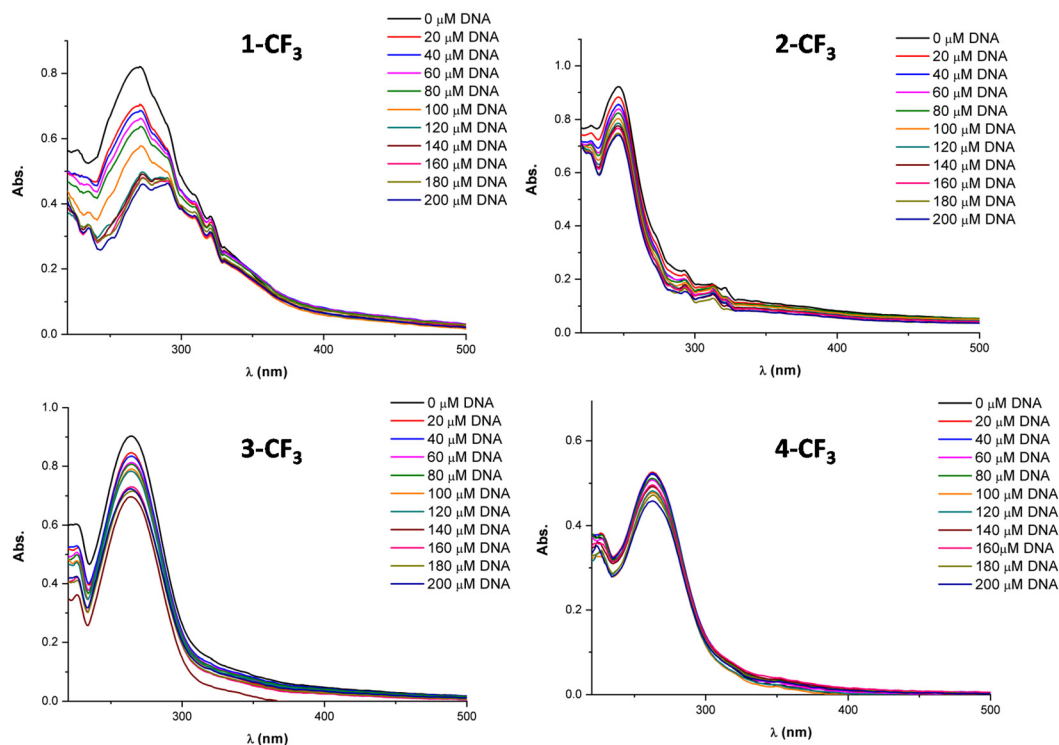
Fig. 5 Absorption spectral titration experiment for complexes **1-CF₃**, **2-CF₃**, **3-CF₃**, and **4-CF₃**.

bases results in a decrease in the energy of the electronic transition $\pi-\pi^*$, leading to bathochromism. Conversely, the π orbitals of the DNA base pairs become partially occupied, reducing the likelihood of the transition and causing hypochromism. Typically, interactions involving intercalation exhibit both hypochromism and bathochromism, although a pronounced red shift is not always observed.

The DNA-binding constants (K_b) determined in this study are on the order of 10^4 M^{-1}, indicating a moderate interaction with DNA. Regarding this aspect, it can be stated that while DNA interaction plays a role in the activity of some of these complexes, it is not the sole factor. Other targets may also contribute to their cytotoxic effects.

Conclusions

Electron-withdrawing substituents in (N^N^N)Pt(pyF) ligands impact photophysical and biological behaviors. Methyl-substituted pyF ligands exhibit notable emission in solution after excitation at ^{1}IL and ^{1}MLCT transitions, as confirmed by TD-DFT calculations. In the solid state, all samples show enhanced phosphorescence emission. The electron nature of the ligand substituents influences singlet oxygen generation. The most potent photosensitizers had CF₃ and Cl groups on the N^N^N ligand. In cytotoxicity studies, family series **2** complexes with specific N^N^N tridentate ligand substituents showed notable cytotoxicity. Under light, their activities generally increase, with fluoromethylated species notably increasing

photocytotoxicity. Complex **2-CF₃** was particularly effective in oxygen production and the phototherapeutic index, while CHF₂-substituted complexes emerged as top photosensitizers. These complexes exhibit moderate DNA binding, likely through intercalation. This interaction probably intensifies under light, aided by singlet oxygen generation. To conclude, the study reveals the importance of electron-based ligand modifications in platinum complexes, shaping their photophysical traits and bioactivity, and hinting at innovative chemotherapeutic and PDT drug designs.

Experimental section

General information

Solvents were purchased from commercial sources and dried by distillation under a nitrogen atmosphere. Reagents 2,6-pyridinedicarbonitrile, 4-chloropyridine-2,6-carbonitrile, *N,N*-diisopropylethylamine (DIPEA), 4-methylpyridine, 4-(trifluoromethyl)pyridine, 4-(difluoromethyl)pyridine, hydrazine hydrate, *p*-toluoyl chloride, and trifluoroacetic acid were purchased from commercial sources and used without further purification. The [PtCl₂(DMSO)₂] precursor was prepared following the procedure described in the literature.[43]

Physical measurements

Infrared spectra were recorded on an FT-IR 520 Nicolet spectrophotometer. ^{1}H NMR (δ(TMS) = 0.0 ppm), ^{19}F NMR (δ(CFCl₃) = 0.0 ppm), and ^{31}P NMR (δ(85% H₃PO₄) = 0.0 ppm) spectra were

obtained on Bruker 400 and Bruker 500 (Universitat de Barcelona) instruments. High resolution electrospray mass spectra (+) were recorded on a Fisons VG Quatro spectrometer (Universitat de Barcelona). Absorption spectra were recorded in a 2 mm or 4 mm quartz cuvette in DMSO on a Cary 5000 UV–Vis–NIR or Shimadzu UV-2450 spectrophotometer. The emission spectra of the compounds in solution were recorded in a fluorescence quartz cuvette of 2 mm or 4 mm length path using a Horiba–Jobin–Yvon SPEX Nanolog spectrofluorimeter. Emission quantum yields were determined with a Hamamatsu Quantaurus QY absolute photoluminescence quantum yield spectrometer C11347. Luminescence lifetimes were measured on JYF-DELTAPRO-NL equipment upon excitation of the samples with a 390 nm NanoLED and collecting the decays through a band pass filter of 550 nm.

Singlet oxygen quantum yield measurements

Room-temperature singlet oxygen phosphorescence was detected at 1270 nm with a Horiba Jobin Yvon SPEX Nanolog spectrofluorometer (Universitat de Barcelona) using the DSS-IGA020L detector. The use of a Schott RG 1000 filter was essential to eliminate from the infrared signal all the first harmonic contributions of sensitizer emission in the region below 850 nm. The singlet oxygen formation quantum yield was then determined by direct measurement of phosphorescence at 1270 nm following irradiation of the aerated aqueous solution of the samples. The samples were adjusted to an absorption of nearly 1 concerning the excitation wavelength to increase the sensitivity of the detection.

Theoretical calculations

The geometries of the complexes were fully optimized without symmetry constraints at the CAM-B3LYP[44]/def2-TZVP[45,46] level of theory by means of the Gaussian-09 program.[47] The basis set includes scalar relativistic effects for Pt in the definition of the ECPs.[46] Solvent effects were taken into consideration using the PCM method[48] as implemented in the Gaussian-16 program.[49] The TD-DFT calculations were computed using 20 excited states at the CAM-B3LYP(solvent = DMSO)/def2-TZVP level of theory using the Gaussian-16 program.

Cell culture

The human lung carcinoma A549 cell line (from the ATCC, USA) was cultured in high glucose Dulbecco's modified Eagle's medium (DMEM) supplemented with 10% fetal bovine serum (FBS) as well as L-glutamine and penicillin/streptomycin at 37 °C under a humidified atmosphere of 95% air and 5% CO$_2$.

Cell viability assays

Cell metabolic activity was analyzed by an MTT-reduction assay to assess the A549 cell sensitivity to the complexes. Thus, 4000 cells (A549) per mL were seeded in flat-bottom 96-well plates (100 μL per well) in complete medium and allowed to attach for 24 h. A stock solution of the complexes was prepared in 0.1 M DMSO. Subsequent dilutions of the different stock solutions from the complexes using DMEM were prepared.

100 μL per well were added to the cells at concentrations ranging from 0.2 to 50 μM (final concentration: 0.1% DMSO); each concentration was performed in quadruplicate. After 1 h or 24 h of incubation with the complexes, duplicates of each concentration were irradiated with an LED lamp of 405 nm with a light dose of 6.5 and 15.1 J m^{-2}, respectively, for 10 min. The cells were cultured for a total of 72 h. 10 μL of MTT (5 mg ml^{-1} in PBS) were added to each well and then further 2 h incubation was allowed at 37 °C. Finally, after removing the culture medium, DMSO (100 μL per well) was added to dissolve the formazan crystals. A 96-well FLUOstar Omega (BMG LABTECH) was used to determine the optical density at 550 nm, and the IC$_{50}$ was calculated. Each experiment was repeated in at least three independent analyses.

DNA binding

The complexes were dissolved in DMSO and diluted with PBS buffer (10 mM, pH = 7.4). The absorption spectra were recorded in a fixed concentration of metal complexes (20 μM) while gradually increasing the concentration of CT-DNA from 0 to 200 μM. To obtain the absorption spectra, the required amount of CT-DNA was added to both the compound solution and the reference solution to eliminate the absorbance of CT-DNA itself. Each sample solution was allowed to equilibrate for 5 min before the spectra were recorded with a Thermo Scientific Evolution 6000. Using the absorption titration data, the binding constant K_b was determined using the Wolfe–Shimer equation:

$$\frac{[DNA]}{(\varepsilon_a - \varepsilon_f)} = \frac{[DNA]}{(\varepsilon_a - \varepsilon_f)} + \frac{1}{K_b(\varepsilon_b - \varepsilon_f)}$$

where [DNA] is the concentration of CT-DNA, ε_a corresponds to the extinction coefficient observed ($A_{obsd}/[M]$), ε_f corresponds to the coefficient of the free compound, ε_b is the extinction coefficient of the compound fully bound to CT-DNA, and K_b is the intrinsic binding constant. The K_b value was given by the ratio of the slope to the intercept in the plot of [DNA]/($\varepsilon_a - \varepsilon_f$) versus [DNA].

Synthesis and characterization

Synthesis of [Pt(L^1)(PyCF$_3$)], 1-CF$_3$. 20 mg (0.30 mmol) of [Pt(DMSO)L^1] were suspended in 5 mL of dry acetonitrile under a nitrogen atmosphere and under reflux. The suspension was stirred for 10 minutes. Then, 4.42 mg (0.30 mmol) of 4-(trifluoromethyl)pyridine were dissolved in 1 mL of acetonitrile and added to the suspension. The reaction was stirred overnight at 65 °C. All the volatiles were then evaporated under vacuum to dryness and the crude product was dissolved in 2 mL of dry DCM and precipitated with an excess of dry hexane. After filtration, a pale-yellow solid was obtained as the final product (15.2 mg, 69% yield). ^{1}H NMR (500 MHz, DMSO-d_6) δ = 8.88 (d, J = 5.7 Hz, 2H), 7.93 (dd, J = 7.6 Hz, 5H), 7.81 (d, J = 8.2 Hz, 2H), 7.72 (d, J = 5.1 Hz, 1H), 7.23 (dd, J = 7.8 Hz, 5H), 2.37–2.34 (m, 6H) ppm. ^{19}F NMR (471 MHz, DMSO-d_6) δ = −63.5 (s, 3F) ppm. ESI (m/z): 733.1525 ([M + H$^+$]$^+$, calcd m/z 733.1527), 717.0160 ([M − CH$_3$ + H$^+$]$^+$, calcd m/z 717.0257),

694.0354 ([M − 2F + H$^+$]$^+$, calcd m/z 694.0521). IR (cm^{-1}): ν = 3031 (C–H$_{ar}$), 2917 (C–H), 1615 (C–N), 1470 (C=C) 1183 (–CF$_3$), 827 (Pt–N).

Synthesis of [Pt(L^1)(PyCHF$_2$)], 1-CHF$_2$. A similar procedure used for **1-CF$_3$** was followed in the synthesis of **1-CHF$_2$** but using 4-(difluoromethyl)pyridine (3.88 mg) instead of 4-(trifluoromethyl)pyridine. A pale-yellow solid was obtained after filtration (9.3 mg, 44% yield). ^{1}H NMR (500 MHz, CDCl$_3$) δ = 10.07 (d, J = 6.5 Hz, 1H), 98.79 (d, J = 6.9 Hz, 5H), 8.04 (d, J = 5.2 Hz, 5H), 7.63 (s, 4H), 6.95–6.65 (m, 1H), 2.38 (s, 6H) ppm. ^{19}F NMR (471 MHz, CDCl$_3$) δ = −63.5 (s, 2F) ppm. ESI (m/z): 716.1624 ([M + H$^+$]$^+$, calcd m/z 716.1661), 666.1364 ([M + 2H$^+$ − CHF$_2$]$^+$, calcd m/z 666.1363). IR (cm^{-1}): ν = 3056 (C–H$_{ar}$), 2917 (C–H), 1615 (C–N), 1061 (C–F), 827 (Pt–N).

Synthesis of [Pt(L^1)(PyCH$_3$)], 1-CH$_3$. A similar procedure used for **1-CF$_3$** was followed in the synthesis of **1-CH$_3$** but using 4-methylpyridine (2.76 mg) instead of 4-(trifluoromethyl) pyridine. A pale-green solid was obtained after filtration (12.3 mg, 60% yield). ^{1}H NMR (400 MHz, DMSO-d_6) δ = 8.33 (s, 4H), 7.97 (s, 3H), 7.24 (d, J = 11.9 Hz, 8H), 2.33 (d, J = 1.9 Hz, 9 H) ppm. ESI (m/z): 680.1833 ([M + H$^+$]$^+$, calcd m/z 680.1835). IR (cm^{-1}): ν = 3015 (C–H$_{ar}$), 2945 (C–H), 1615 (C–N), 1472 (C=C), 745 (Pt–N).

Synthesis of [Pt(L^2)(PyCF$_3$)], 2-CF$_3$. A similar procedure used for **1-CF$_3$** was followed in the synthesis of **2-CF$_3$** but using [Pt(DMSO)L^2] (4.20 mg) instead of [Pt(DMSO)L^1]. A pale brown solid was obtained after filtration (18.5 mg, 84% yield). ^{1}H NMR (500 MHz, CDCl$_3$) δ = 10.38 (s, 2H), 9.48–8.81 (m, 1H), 8.29–7.92 (m, 1H), 7.93–7.76 (m, 5H), 7.42–7.26 (m, 5H), 2.38 (s, 6H) ppm. ^{19}F NMR (471 MHz, CDCl$_3$) δ = −63.9 (s, 3F) ppm. ESI (m/z): 782.0509 ([M + NH$_4^+$]$^+$, calcd m/z 782.0512). IR (cm^{-1}): ν = 3062 (C–H$_{ar}$), 2923 (C–H), 1666 (C–N), 1137 (–CF$_3$), 843 (Pt–N), 728 (C–Cl).

Synthesis of [Pt(L^2)(PyCHF$_2$)], 2-CHF$_2$. A similar procedure used for **2-CF$_3$** was followed in the synthesis of **2-CHF$_2$** but using 4-(difluoromethyl)pyridine (3.69 mg) instead of 4-(trifluoromethyl)pyridine. A pale-brown solid was obtained after filtration (17.8 mg, 83% yield). ^{1}H NMR (500 MHz, DMSO-d_6) δ = 8.88 (s, 4H), 8.26 (m 2H), 8.11 (d, J = 6.5 Hz, 1H), 7.96 (d, J = 6.8 Hz, 1H), 7.90 (d, J = 6.8 Hz, 3H), 7.83–7.78 (m, 4H), 7.23–7.13 (m, 1H), 2.53 (s, 6H) ppm. ^{19}F NMR (471 MHz, DMSO-d_6) δ = −63.4 (s, 2F) ppm. ESI (m/z): 764.0622 ([M + NH$_4^+$]$^+$, calcd m/z 764.0627), 695.2037 ([M − CHF$_2$ + H$^+$]$^+$, calcd m/z 695.2039). IR (cm^{-1}): 3002 (C–H$_{ar}$), 2920 (C–H), 1628 (C–N), 1052 (C–F), 811 (Pt–N), 738 (C–Cl).

Synthesis of [Pt(L^2)(PyCH$_3$)], 2-CH$_3$. A similar procedure used for **2-CF$_3$** was followed in the synthesis of **2-CH$_3$** but using 4-methylpyridine (3.69 mg) instead of 4-(trifluoromethyl) pyridine. A pale-brown solid was obtained after filtration (9.6 mg, 48% yield). ^{1}H NMR (500 MHz, CDCl$_3$) δ = 9.21 (s, 2H), 8.84–8.68 (m, 1H), 8.64–8.58 (m, 1H), 7.88–7.80 (m, 4H), 7.75 (d, J = 6.0 Hz, 1H), 7.34–7.37 (m, 4H), 7.26–7.15 (m, 1H), 2.50 (s, 6H), 2.48 (d, J = 15.0 Hz, 3H) ppm. ESI (m/z): 743.1697 ([M + 2NH$_4^+$]$^+$, calcd m/z 743.1701). IR (cm^{-1}): 3050 (C–H$_{ar}$), 2996 (C–H), 1625 (C–N), 1498 (C=C), 1429 (–CH$_3$), 824 (Pt–N), 745 (C–Cl).

Synthesis of [Pt(L^3)(PyCF$_3$)], 3-CF$_3$. A similar procedure used for **1-CF$_3$** was followed in the synthesis of **3-CF$_3$** but using [Pt(DMSO)L^3] (4.73 mg) instead of [Pt(DMSO)L^1]. A pale brown solid was obtained after filtration (9.6 mg, 43% yield). ^{1}H NMR (500 MHz, DMSO-d_6) δ = 8.89 (ddd, J = 4.4, 1.6, 0.7 Hz, 2H), 8.46–8.38 (m, 1H), 8.12 (d, J = 8.0 Hz, 1H), 7.91 (d, J = 7.9 Hz, 1H), 7.82–7.76 (m, 2H) ppm. ^{19}F NMR (471 MHz, DMSO-d_6) δ −63.2 (s, 3F), −62.8 (s, 6F), ppm. ESI (m/z): 643.0023 ([M − CF$_3$ + Na$^+$]$^+$, calcd m/z 643.0026), 621.0198 ([M − CF$_3$]$^+$, calcd m/z 621.0201). IR (cm^{-1}): ν = 3052 (C–H$_{ar}$), 2976 (C–H), 2495 (N–CH), 1654 (C–N), 1476 (C=C), 1154 (–CF$_3$), 813 (Pt–N).

Synthesis of [Pt(L^3)(PyCHF$_2$)], 3-CHF$_2$. A similar procedure used for **3-CF$_3$** was followed in the synthesis of **3-CHF$_2$** but using 4-(difluoromethyl)pyridine (4.15 mg) instead of 4-(trifluoromethyl)pyridine. A pale brown solid was obtained after filtration (12.5 mg, 58% yield). ^{1}H NMR (500 MHz, CDCl$_3$) δ = 9.98–9.92 (m, 2H), 8.08 (dd, J = 8.3, 7.7 Hz, 1H), 7.88 (d, J = 7.9 Hz, 3H), 7.82 (d, J = 6.1 Hz, 2H), 6.78 (t, J = 55.0 Hz, 1H) ppm. ^{19}F NMR (471 MHz, CDCl$_3$) δ = −64.3 ppm (s, 9F). ESI (m/z): 696.1039 ([M + Na$^+$]$^+$, calcd m/z 696.1041), 673.0448 ([M + H$^+$]$^+$, calcd m/z 673.0457), 642.0040 ([M − CHF$_2$ + Na$^+$]$^+$, calcd m/z 642.0046), 621.0022 ([M − CHF$_2$ + H$^+$]$^+$, calcd m/z 621.0029). IR (cm^{-1}): 3074 (C–H$_{ar}$), 2940 (C–H), 2491 (N–CH), 1632 (C–N), 1160 (–CF$_3$), 1005 (C–F), 824 (Pt–N).

Synthesis of [Pt(L^3)(PyCH$_3$)], 3-CH$_3$. A similar procedure used for **3-CF$_3$** was followed in the synthesis of **3-CH$_3$** but using 4-methylpyridine (2.99 mg) instead of 4-(trifluoromethyl) pyridine. A pale brown solid was obtained after filtration (8.7 mg, 43% yield). ^{1}H NMR (500 MHz, CDCl$_3$) δ = 9.53–9.47 (m, 2H), 8.06 (t, J = 7.9 Hz, 1H), 7.87 (d, J = 7.9 Hz, 2H), 7.49–7.43 (m, 2H), 2.54 (s, 3H) ppm. ^{19}F NMR (471 MHz, CDCl$_3$) δ = −64.3 (s, 6F) ppm. ESI (m/z): 659.1185 ([M + Na$^+$]$^+$, calcd m/z 659.1181), 636.0648 ([M + H$^+$]$^+$, calcd m/z 636.0649). IR (cm^{-1}): ν = 3034 (C–H$_{ar}$), 2948 (C–H), 2372 (N–CH), 1634 (C–N), 1125 (–CF$_3$), 814 (Pt–N).

Synthesis of [Pt(L^4)(PyCF$_3$)], 4-CF$_3$. A similar procedure used for **1-CF$_3$** was followed in the synthesis of **4-CF$_3$** but using [Pt(DMSO)L^4] (4.48 mg) instead of [Pt(DMSO)L^1]. A pale red solid was obtained after filtration (9.4 mg, 42% yield). ^{1}H NMR (400 MHz, DMSO-d_6) δ = 8.88 (d, J = 5.1 Hz, 1H), 8.75 (s, 1H), 8.21 (s, 2H), 8.11 (s, 1H), 7.79 (d, J = 5.2 Hz, 1H) ppm. ^{19}F NMR (376 MHz, DMSO-d_6) δ = −62.8 (s, 6F), −63.1 (s, 3F) ppm. ESI (m/z): 758.2189 ([M + Na$^+$]$^+$, calcd m/z 758.2198), 684.0234 ([M − Cl]$^+$, calcd m/z 684.0236). IR (cm^{-1}): ν = 3088 (C–H$_{ar}$), 2958 (C–H), 1637 (C–N), 1318 (C=C), 1150 (–CF$_3$), 833 (Pt–N), 789 (C–Cl).

Synthesis of [Pt(L^4)(PyCHF$_2$)], 4-CHF$_2$. A similar procedure used for **4-CF$_3$** was followed in the synthesis of **4-CHF$_2$** but using 4-(difluoromethyl)pyridine (3.93 mg) instead of 4-(trifluoromethyl)pyridine. A pale-yellow solid was obtained after filtration (14.7 mg, 68% yield). ^{1}H NMR (500 MHz, DMSO-d_6) δ = 8.76 (d, J = 5.8 Hz, 2H), 8.40 (s, 1H), 8.11 (s, 1H), 7.57 (d, J = 5.2 Hz, 2H), 7.26–6.93 (m, 1H) ppm. ^{19}F NMR (471 MHz, DMSO-d_6) δ = −62.8 (s, 6F), −63.2 (s, 3F) ppm. ESI (m/z): 706.0069 ([M + H$^+$]$^+$, calcd m/z 706.0075), 677.9313 ([M − CHF$_2$ + Na$^+$]$^+$, calcd m/z 677.9364). IR (cm^{-1}): 2998 (C–H$_{ar}$), 1618

(C–N), 1448 (C=C), 1133 (–CF$_3$), 1001 (C–F), 822 (Pt–N), 745 (C–Cl).

Synthesis of [Pt(L^4)(PyCH$_3$)], 4-CH$_3$. A similar procedure used for **3-CH$_3$** was followed in the synthesis of **4-CH$_3$** but using 4-methylpyridine (2.84 mg) instead of 4-(trifluoromethyl) pyridine. A pale-yellow solid was obtained after filtration (9.5 mg, 47% yield). ^{1}H NMR (500 MHz, CDCl$_3$) δ = 9.51 (d, J = 6.1 Hz, 2H), 7.90 (s, 2H), 7.50–7.45 (m, 2H), 2.55 (s, 3H) ppm. ^{19}F NMR (471 MHz, CDCl$_3$) δ = −64.3 (s, 6F) ppm. ESI (m/z): 636.0636 ([M − Cl + H$^+$]$^+$, calcd m/z 636.0633), 568.4215 ([M − C$_6$H$_7$N + H$^+$]$^+$, calcd m/z 568.4612). IR (cm^{-1}): ν = 3088 (C–H$_{ar}$), 2948 (C–H), 2486 (N–CH), 1631 (C–N), 1121 (–CF$_3$), 814 (Pt–N), 748 (C–Cl).

Conflicts of interest

There are no conflicts to declare.

Acknowledgements

References

1 M. Mauro, A. Aliprandi, D. Septiadi, N. S. Kehr and L. De Cola, *Chem. Soc. Rev.*, 2014, **43**, 4144–4166.

2 M. Casciotti, G. Romo-Islas, M. Álvarez, F. Molina, J. M. Muñoz-Molina, T. R. Belderrain and L. Rodríguez, *Dalton Trans.*, 2022, **51**, 17162–17169.

3 A. Haque, L. Xu, R. A. Al-Balushi, M. K. Al-Suti, R. Ilmi, Z. Guo, M. S. Khan, W. Y. Wong and P. R. Raithby, *Chem. Soc. Rev.*, 2019, **48**, 5547–5563.

4 M. Albrecht and G. Van Koten, *Angew. Chem., Int. Ed.*, 2001, **40**, 3750–3781.

5 M. J. Bryant, J. M. Skelton, L. E. Hatcher, C. Stubbs, E. Madrid, A. R. Pallipurath, L. H. Thomas, C. H. Woodall, J. Christensen, S. Fuertes, T. P. Robinson, C. M. Beavers, S. J. Teat, M. R. Warren, F. Pradaux-Caggiano, A. Walsh, F. Marken, D. R. Carbery, S. C. Parker, N. B. McKeown,

R. Malpass-Evans, M. Carta and P. R. Raithby, *Nat. Commun.*, 2017, **8**, 1800.

6 M. C. Derosa and R. J. Crutchley, *Coord. Chem. Rev.*, 2002, **233–234**, 351–371.

7 J. Bonelli, E. Ortega-Forte, A. Rovira, M. Bosch, O. Torres, C. Cuscó, J. Rocas, J. Ruiz and V. Marchán, *Biomacromolecules*, 2022, **23**, 2900–2913.

8 L. Wang, J. Karges, F. Wei, L. Xie, Z. Chen, G. Gasser, L. Ji and H. Chao, *Chem. Sci.*, 2023, **14**, 1461–1471.

9 R. Ossola, O. M. Jönsson, K. Moor and K. McNeill, *Chem. Rev.*, 2021, **121**, 4100–4146.

10 C. Colomban, V. Martin-Diaconescu, T. Parella, S. Goeb, C. García-Simón, J. Lloret-Fillol, M. Costas and X. Ribas, *Inorg. Chem.*, 2018, **57**, 3529–3539.

11 F. Heinemann, J. Karges and G. Gasser, *Acc. Chem. Res.*, 2017, **50**, 2727–2736.

12 H. Huang, S. Banerjee and P. J. Sadler, *ChemBioChem*, 2018, **19**, 1574–1589.

13 L. Huang, M. Rudolph, F. Rominger and A. S. K. Hashmi, *Angew. Chem.*, 2016, **128**, 4888–4893.

14 A. Pinto, A. Llanos, R. M. Gomila, A. Frontera and L. Rodríguez, *Inorg. Chem.*, 2023, **62**, 7131–7140.

15 G. Romo-Islas, J. S. Ward, K. Rissanen and L. Rodríguez, *Inorg. Chem.*, 2023, **62**, 8101–8111.

16 M. Yang, J. Deng, D. Guo, J. Zhang, L. Yang and F. Wu, *Org. Biomol. Chem.*, 2019, **17**, 5367–5374.

17 G. K. Couto, B. S. Pacheco, V. M. Borba, J. C. R. Junior, T. L. Oliveira, N. V. Segatto, F. K. Seixas, T. V. Acunha, B. A. Iglesias and T. Collares, *J. Photochem. Photobiol., B*, 2020, **202**, 111725.

18 A. Lázaro, C. Cunha, R. Bosque, J. Pina, J. S. Ward, K. N. Truong, K. Rissanen, J. C. Lima, M. Crespo, J. S. Seixas De Melo and L. Rodríguez, *Inorg. Chem.*, 2020, **59**, 8220–8230.

19 M. Li, Y. Xu, M. Zhao, F. Li, W. Feng, T. Feng, S. Liu and Q. Zhao, *Inorg. Chem.*, 2020, **59**, 17826–17833.

20 A. Salim Abu-Surrah and M. Kettunen, *Curr. Med. Chem.*, 2006, **13**, 1337–1357.

21 Z. Xie, T. Fan, J. An, W. Choi, Y. Duo, Y. Ge, B. Zhang, G. Nie, N. Xie, T. Zheng, Y. Chen, H. Zhang and J. S. Kim, *Chem. Soc. Rev.*, 2020, **49**, 8065–8087.

22 K. Jayanetti, K. Takemura, H. Bendale, A. Garg and I. Ojima, *J. Fluorine Chem.*, 2023, **267**, 110106.

23 G. Romo-Islas, R. M. Gomila, A. Frontera and L. Rodríguez, *Inorg. Chem. Front.*, 2023, **10**, 6204–6220.

24 M. Mydlak, M. Mauro, F. Polo, M. Felicetti, J. Leonhardt, G. Diener, L. De Cola and C. A. Strassert, *Chem. Mater.*, 2011, **23**, 3659–3667.

25 S. C. Gangadharappa, I. Maisuls, I. P. Salto, S. Niemann, V. Bachtin, F. C. Herrmann and C. A. Strassert, *J. Phys. Chem. C*, 2021, **125**, 5739–5747.

26 D. Septiadi, A. Aliprandi, M. Mauro and L. De Cola, *RSC Adv.*, 2014, **4**, 25709–25718.

27 Y. Li, K. M. C. Wong, H. L. Wong and V. W. W. Yam, *ACS Appl. Mater. Interfaces*, 2016, **8**, 17445–17453.

28 L. Stegemann, J. Sanning, C. G. Daniliuc and C. A. Strassert, *Z. Naturforsch., B: J. Chem. Sci.*, 2016, **71**, 1087–1093.

29 S. Chakraborty, A. Aliprandi and L. De Cola, *Chem. – Eur. J.*, 2020, **26**, 11007–11012.

30 S. Sinn, F. Biedermann, M. Vishe, A. Aliprandi, C. Besnard, J. Lacour and L. De Cola, *ChemPhysChem*, 2016, 1829–1834.

31 A. Ruiz-Carretero, Y. Atoini, T. Han, A. Operamolla, S. Ippolito, C. Valentini, S. Carrara, S. Sinn, E. A. Prasetyanto, T. Heiser, P. Samorì, G. Farinola and L. De Cola, *J. Mater. Chem. A*, 2019, **7**, 16777–16784.

32 A. Aliprandi, D. Genovese, M. Mauro and L. De Cola, *Chem. Lett.*, 2015, **44**, 1152–1169.

33 A. Lázaro, R. Bosque, J. S. Ward, K. Rissanen, M. Crespo and L. Rodríguez, *Inorg. Chem.*, 2023, **62**, 2000–2012.

34 C. Lochenie, A. Insuasty, T. Battisti, L. Pesce, A. Gardin, C. Perego, M. Dentinger, D. Wang, G. M. Pavan, A. Aliprandi and L. De Cola, *Nanoscale*, 2020, **12**, 21359–21367.

35 S. Sinn, F. Biedermann and L. De Cola, *Chem. – Eur. J.*, 2017, **23**, 1965–1971.

36 R. Soldati, A. Alipri, M. Mauro, L. De Cola and D. Giacomini, *Eur. J. Org. Chem.*, 2014, 7113–7121.

37 S. Goswami, R. W. Winkel and K. S. Schanze, *Inorg. Chem.*, 2015, **54**, 10007–10014.

38 I. Toubia, C. Nguyen, S. Diring, L. M. A. Ali, L. Larue, R. Aoun, C. Frochot, M. Gary-Bobo, M. Kobeissi and F. Odobel, *Inorg. Chem.*, 2019, **58**, 12395–12406.

39 S. W. Lai, Y. Liu, D. Zhang, B. Wang, C. N. Lok, C. M. Che and M. Selke, *Photochem. Photobiol.*, 2010, **86**, 1414–1420.

40 E. Ortega, C. Pérez-Arnaiz, V. Rodríguez, C. Janiak, N. Busto, B. García and J. Ruiz, *Eur. J. Med. Chem.*, 2021, **222**, 113600.

41 A. Lázaro, C. Cunha, R. Bosque, J. Pina, J. S. Ward, K. N. Truong, K. Rissanen, J. C. Lima, M. Crespo, J. S. Seixas De Melo and L. Rodríguez, *Inorg. Chem.*, 2020, **59**, 8220–8230.

42 M. Jóźwiak, M. Struga, P. Roszkowski, A. Filipek, G. Nowicka and W. Olejarz, *Biomed. Pharmacother.*, 2019, **110**, 618–630.

43 J. H. Price, A. N. Williamson, R. F. Schramm and B. B. Wayland, *Inorg. Chem.*, 1972, **11**, 1280–1284.

44 T. Yanai, D. Tew and N. Handy, *Chem. Phys. Lett.*, 2004, **393**, 51–57.

45 F. Weigend and R. Ahlrichs, *Phys. Chem. Chem. Phys.*, 2005, **7**, 3297–3305.

46 F. Weigend, *Phys. Chem. Chem. Phys.*, 2006, **8**, 1057–1065.

47 M. J. Frisch, *et al.*, *Gaussian 09 (Revision D.1)*, Gaussian Inc., Wallingford CT, 2010.

48 J. Tomasi, B. Mennucci and R. Cammi, *Chem. Rev.*, 2005, **105**, 2999–3093.

49 M. J. Frisch, G. W. Trucks, H. B. Schlegel, G. E. Scuseria, M. A. Robb, J. R. Cheeseman, G. Scalmani, V. Barone, G. A. Petersson, H. Nakatsuji, X. Li, M. Caricato, A. V. Marenich, J. Bloino, B. G. Janesko, R. Gomperts, B. Mennucci, H. P. Hratchian, J. V. Ortiz, A. F. Izmaylov, J. L. Sonnenberg, D. Williams-Young, F. Ding, F. Lipparini, F. Egidi, J. Goings, B. Peng, A. Petrone, T. Henderson, D. Ranasinghe, V. G. Zakrzewski, J. Gao, N. Rega, G. Zheng, W. Liang, M. Hada, M. Ehara, K. Toyota, R. Fukuda, J. Hasegawa, M. Ishida, T. Nakajima, Y. Honda, O. Kitao, H. Nakai, T. Vreven, K. Throssell, J. A. Montgomery Jr., J. E. Peralta, F. Ogliaro, M. J. Bearpark, J. J. Heyd, E. N. Brothers, K. N. Kudin, V. N. Staroverov, T. A. Keith, R. Kobayashi, J. Normand, K. Raghavachari, A. P. Rendell, J. C. Burant, S. S. Iyengar, J. Tomasi, M. Cossi, J. M. Millam, M. Klene, C. Adamo, R. Cammi, J. W. Ochterski, R. L. Martin, K. Morokuma, O. Farkas, J. B. Foresman and D. J. Fox, *Gaussian 16, Revision A.01*, Gaussian, Inc., Wallingford CT, 2016.